Journal of Nanobiotechnology

RESEARCH Open Access

Titanium nanoparticles released from orthopedic implants induce muscle fibrosis via activation of SNAI2

Gengming Zhang[1,2†], Linhua Deng[1,2†], Zhongjing Jiang[1,2], Gang Xiang[1,2], Zhuotong Zeng[3,4], Hongqi Zhang[1,2] and Yunjia Wang[1,2*]

Abstract

Titanium alloys represent the prevailing material employed in orthopedic implants, which are present in millions of patients worldwide. The prolonged presence of these implants in the human body has raised concerns about possible health effects. This study presents a comprehensive analysis of titanium implants and surrounding tissue samples obtained from patients who underwent revision surgery for therapeutic reasons. The surface of the implants exhibited nano-scale corrosion defects, and nanoparticles were deposited in adjacent samples. In addition, muscle in close proximity to the implant showed clear evidence of fibrotic proliferation, with titanium content in the muscle tissue increasing the closer it was to the implant. Transcriptomics analysis revealed SNAI2 upregulation and activation of PI3K/AKT signaling. In vivo rodent and zebrafish models validated that titanium implant or nanoparticles exposure provoked collagen deposition and disorganized muscle structure. Snai2 knockdown significantly reduced implant-associated fibrosis in both rodent and zebrafish models. Cellular experiments demonstrated that titanium dioxide nanoparticles (TiO_2 NPs) induced fibrotic gene expression at sub-cytotoxic doses, whereas Snai2 knockdown significantly reduced TiO_2 NPs-induced fibrotic gene expression. The in vivo and in vitro experiments collectively demonstrated that Snai2 plays a pivotal role in mediating titanium-induced fibrosis. Overall, these findings indicate a significant release of titanium nanoparticles from the implants into the surrounding tissues, resulting in muscular fibrosis, partially through Snai2-dependent signaling.

†Gengming Zhang and Linhua Deng contributed equally to this work.

*Correspondence:
Yunjia Wang
yunjia_wang@csu.edu.cn

Full list of author information is available at the end of the article

Graphical Abstract

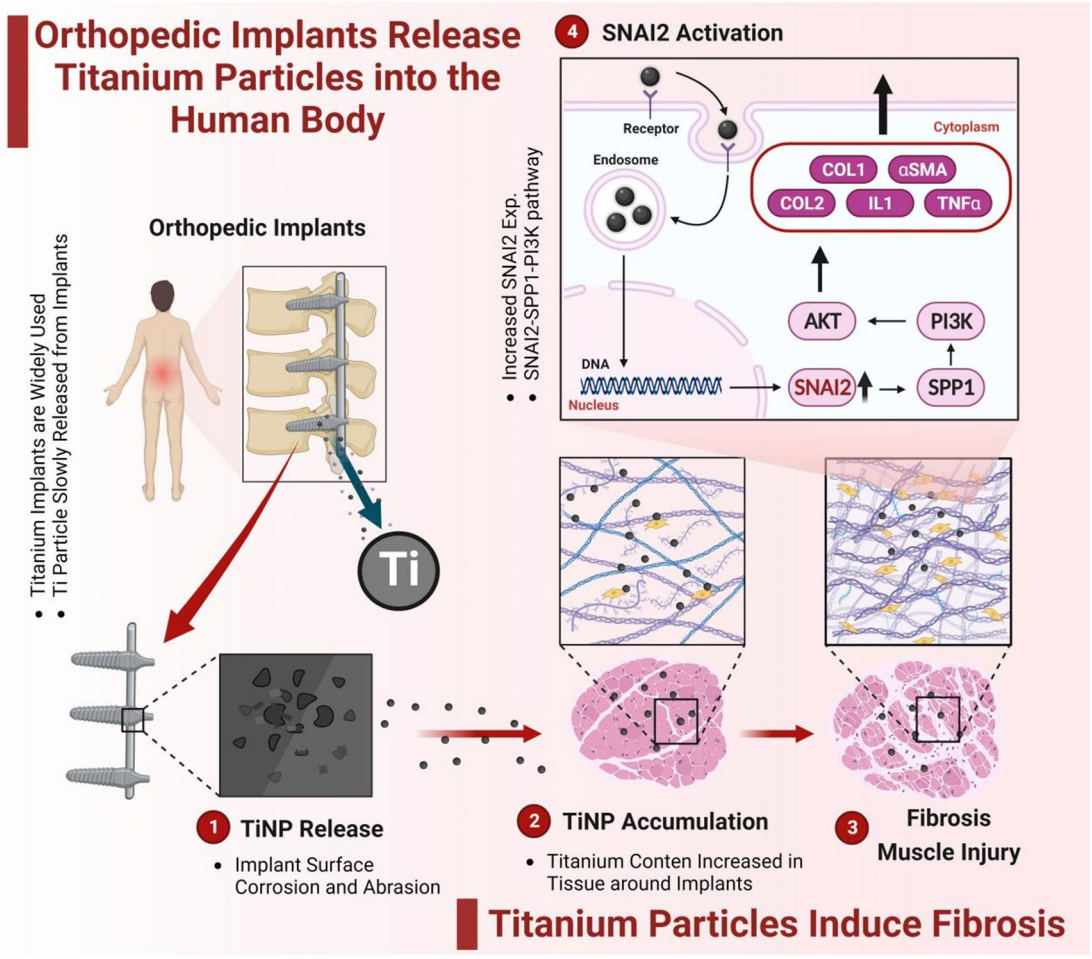

Keywords Orthopedic implants, Titanium, Titanium dioxide nanoparticles, Muscle fibrosis, SNAI2

Introduction

Titanium alloys have become a cornerstone in the preparation of orthopedic and dental implants in the field of biomedical materials due to their excellent mechanical properties, including strength, rigidity, and corrosion resistance [1, 2]. These properties enable them to effectively adapt to physiological loads and meet the requirements for orthopedic and dental restoration in terms of mechanical performance, corrosion resistance, and biosafety compatibility [3, 4]. The demand for titanium alloy biomedical materials is expected to continue growing in the future due to the increasing number of orthopedic surgeries worldwide, which exceeds 3 million annually, and the estimated use of over 1,000 tons of medical titanium implants [5]. There are concerns about the potential toxicity of some titanium implants that remain in the body for long periods of time, undergoing wear and corrosion [6, 7]. Long-term exposure to titanium implants may cause metal overload and complications, such as peri-implantitis and osteolysis [8, 9]. It has been reported that extended contact with titanium implants can lead to fibrosis of muscles and connective tissues in the vicinity of the implant [9]. However, the precise mechanism by which this occurs remains unclear. Consequently, it is vital to assess the impact of titanium implants on surrounding muscle tissue to inform further therapeutic and prophylactic strategies.

In general, titanium alloys are usually considered to be safer materials for use in implants. However, recent studies have indicated that titanium implants can induce a range of in vivo toxicities, including neurotoxicity, muscular toxicity, and hepatorenal toxicity [9–11]. Studies on the mechanisms of toxicity suggest that the release of particles and ions from the implant

surface may be a mediator of their toxic effects [12, 13]. Titanium implants have the potential to release microparticles. This is primarily due to corrosion, abrasion, and oxidation processes that occur on the surface of titanium alloys [14]. Their mode of action involves direct contact with the tissue surrounding the implant, triggering various biological responses such as fibrosis. Myocardial fibrosis may result from prolonged exposure to TiO_2 NPs [15]. In addition, TiO_2 NPs can be transported over long distances by multiple pathways, such as blood flow and nerve cells, for deposition in target organs and corresponding pathologic changes [16]. It has been shown that there is evidence of TiO_2 NPs in the nervous system after exposure to titanium implants [17]. Deposition of TiO_2 NPs in the brain may cause neurological damage.

The toxicity mechanism of TiO_2 NPs involves multiple pathways, including inducing inflammatory responses, regulating cellular metabolism, and interfering with cellular signaling cascades [18]. Once TiO_2 NPs enter the human body, they enter the cells of tissues and organs through different pathways, such as micropinocytosis and receptor-mediated endocytosis [19]. They activate different gene expressions and cause a variety of cellular damage. Therefore, the related toxicity mechanisms are different and need to be analyzed and studied separately. One of the major effects of titanium particles on the surrounding tissues is to induce tissue fibrosis, and animal experiments have shown that titanium particles can induce fibrosis by activating the expression of TGF-β1 [20]. In vitro investigation demonstrated that exposure to titanium, aluminum, and vanadium ions released from titanium implants elicited dysfunction and redox imbalance within fibroblast mitochondria [21].

In patients who had undergone implantation of long-segment titanium alloys, we discovered the presence of tissue scar hyperplasia and hyperfibrosis surrounding the titanium implants during second revision surgery. Therefore, we hypothesized that prolonged exposure to titanium implants may be the cause of muscle tissue fibrosis. In this study, we examined tissue samples taken from patients who had implants for more than a year and observed significant fibrosis in the specimens. Nanoscale corrosion was observed on the surface of the implant. Nanoscale particles were detected in the tissue surrounding the implant, and the titanium content was significantly elevated. This indicates that titanium nanoparticles were released from the implant surface into the surrounding tissues, which may cause fibrosis of the surrounding tissues. Further studies validated our hypothesis by showing that exposure to titanium implant and nanoparticles in rats and zebrafish could induce fibrosis and muscle damage phenotypes. Mechanistic studies showed that TiO_2 NPs caused an increase in the expression of fibrotic genes, mainly through the Snai2-Spp1-PI3K signaling pathway. This finding elucidates the mechanism of titanium implant-induced fibrosis.

Materials and methods

Ethics statement and human specimen collection

All experimental procedures involving human specimens and animal experimentation were subject to review and approval by the Ethics Committee of Xiangya Hospital, Central South University (Protocol No. 202103372). All included subjects gave their written informed consent to participate in the study. A total of 50 patients (Cohort I for tissue specimen and Cohort II for blood sample) were recruited from Xiangya Hospital. Detailed clinical characteristics of the patient cohort I are presented (Table S1). Inclusion criteria for patients were: At least one year after spinal nail-rod internal fixation with mobilization of more than three vertebral units, no previous surgery at the same site, and no other metal implants in the body. Tissue specimens were collected from 8 patients aged 15–55 years who underwent revision of titanium alloy implants, as well as 8 normal controls aged 13–51 years (Table S1). Muscle and scar tissues surrounding the titanium alloy implants were collected, as well as peripheral blood samples from the patients and samples of the titanium alloy implants removed during the operation.

RNA-seq and bioinformatic analysis

RNA-seq analysis was performed on human tissue samples collected. The library was constructed using Illumina's NEBNext® UltraTM RNA Library Prep Kit and then the Agilent 2100 bioanalyzer was utilized to detect the library's insert size to ensure its quality. Read counts were mapped to each gene via feature Counts. Differential expression analysis was performed between the two comparison groups, each consisting of two biological replicates, using DESeq2 R software (version 1.16.1). Also, we utilized the clusterProfiler R software to examine the statistical enrichment of genes that were expressed differentially in the KEGG pathways.

Characterization of implant

The surface morphology of the titanium alloy and Co-Cr-Mo implant removed from the body were observed using scanning electron microscopy (SEM, ZEISS Sigma 300, Germany). The elemental composition of the titanium alloy implant was analyzed using SEM-EDS. The dominant element in the composition of the titanium implants was titanium, accounting for 89.34%, with Al and V making up 5.46% and 4.96%, respectively The surface electronic state of the Titanium implant was determined by X-ray photoelectron spectroscopy (XPS, Kratos Axis Ultra DLD).

Nanoparticle characterization

Nano-TiO_2 (TiO_2 NPs) and nano- Co_3O_4 (CoNPs) were purchased from Hangzhou Wanjing New Material Co., Ltd. (average diameter 30–50 nanometers; purity ≥ 99.9%). The particle morphology of TiO_2 NPs and CoNPs were observed using scanning electron microscopy (SEM, ZEISS Sigma 300, Germany).

ICP-MS

Accurately weigh the sample in a microwave digestion tube and add 10mL nitric acid. Pre-digest the sample at 120℃ for 30 min before proceeding with microwave digestion. Dilute to 25mL using 1% nitric acid and shake thoroughly for testing. Analyze using the Agilent 7800 (Agilent, Santa Clara, CA, United States).

TEM analysis

The collected human muscle tissue samples surrounding titanium implants and zebrafish tissue samples were preserved in an electron microscopy fixative solution (Servicebio, Wuhan, China). Subsequently, the samples were fixed in 1% osmic acid for 1–2 h. They were then dehydrated through a gradient series of ethanol concentrations (30%, 50%, 70%, 80%, 90%, and 95%). After treatment with acetone, the samples were embedded in embedding medium. Ultrathin sections of 70–90 nm were obtained using a microtome, and were stained with lead citrate solution and 50% ethanol-saturated uranyl acetate solution for 5–10 min each. The dried sections were observed under a Hitachi H-7650 transmission electron microscope (Thermo Fisher Scientific, Waltham, MA).

Zebrafish

The study employed the wild AB strain of zebrafish, acquired from the Institute of Hydrobiology, Chinese Academy of Sciences. Normally developing embryos at the blastocyst stage (2 hpf) were collected. These embryos were randomized and subsequently placed in separate containers. At 2 days post-fertilization (dpf), 500 milliliters of TiO_2 NPs or CoNPs solutions with varying concentrations of 0, 1, 10, 20, 60, 80, and 100 mg/L were added to each container and replaced every 24 h. There were three repetitions for each process. The embryos were incubated at 28 ± 0.5 °C with 14 h of light per day during the experiment. Throughout the experiment, the hatching and mortality rates were monitored every 24 h. The malformation rate of the surviving zebrafish was calculated at 4 dpf, while muscle tissues were collected from each zebrafish group at approximately 9 dpf. In order to build snai2 knock-out zebrafish line, we developed four guideRNAs targeting the *snai2* gene for Cas9 gene knockout [22]. The Cas9 protein complexes were injected into one-cell stage embryo and *snai2* mRNA expression were determined by qPCR to validate knockout efficiency. The larvae were randomly divided into a non- TiO_2 NPs treatment group and a TiO_2 NPs treatment group. The TiO_2 NPs solution was added at 3 dpf and replaced every 24 h. Each treatment was replicated three times. Muscle tissues were collected from each group of zebrafish at approximately 9 dpf.

Rats model

The male SD rats weighing between 300 and 350 g and aged six weeks were utilized to develop a rat model consisting of a titanium alloy implant. The patient derived titanium alloy implant was sterilized and fabricated into a titanium alloy implant plate with a thickness of approximately 1–2 mm. Implants are inserted into the muscle at a depth of 0.2 mm from the subcutaneous area, with a distance of 1–2 cm between implants. A total of 16 SD male rats were chosen for the modeling process and 4 regions on their backs were implanted with the implants. At the same time, snai2 siRNA (Table S5) that was encapsulated in Pluronic F-127 (Sigma-Aldrich, MO, USA) was injected into the implant sites of titanium alloy in eight mice on days 3, 12, and 21. All the animals were kept in a specific pathogen-free (SPF) facility and were housed in polycarbonate cages having standard rodent food and ad-lib water. The light/dark cycle was set to 12/12 hours and the room temperature was maintained at 22.5 °C. All animals were treated with humane care during pain relief procedures, and the Animal Utilization and Chinese Nursing Committee of Central South University approved the experimental protocol. On day 30, rats were sacrificed, and corresponding tissue samples were collected.

Histologcal analyses

The tissue samples obtained in this study (including human, zebrafish, and SD rats) were preserved by fixing them in 10% buffered formaldehyde (pH 7.4) for 24 h to maintain the integrity of the protoplasts. The samples were then dehydrated, embedded in paraffin, and cut into 2.5 μm sections using a rotary microtome. The sections were subjected to dewaxing, hydration, and hematoxylin and eosin staining, followed by Masson staining to observe fibrosis.

Immunohistochemistry

As previously stated, the paraffin sections that were obtained underwent antigen repair and were then exposed to monoclonal antibodies against collagen I (Proteintech, China), SPP1 (Proteintech, China), and SNAI2 (Affinity, China) at 4 °C for an overnight incubation. Following this, the tissue sections were treated with biotinylated goat anti-rabbit antibodies (1:500, Zhongshan Jinqiao) and subsequently underwent signal

generation through the use of diaminobenzidine (DAB) as a substrate.

Immunofluorescence

Rat muscle tissue was utilized to prepare paraffin sections, which were subsequently deparaffinized and had their antigen restored. The sections were then blocked with 5% bovine serum albumin at room temperature for one hour before being incubated overnight at 4 °C with anti-collagen I (Proteintech, China, 1:200), anti-α-SMA (Proteintech, China, 1:3000), anti-SPP1 (Proteintech, China, 1:3000), and anti-SNAI2 (CST, America, 1:1000). The following day, the samples were warmed and then washed with PBS. A fluorescent secondary antibody was introduced, and the samples were incubated in the dark for one hour. Following DAPI staining, the sections were observed using a fluorescence microscope (NIKON ECLIPSE CI, Nikon, Japan).

Cell culture

The mouse myoblast C2C12 and mouse fibroblast L-929 cell lines utilized in this investigation were acquired from Procell (Procell, Wuhan, China). C2C12 cells were maintained in DMEM (Procell, Wuhan, PM150312, China) supplemented with 10% fetal bovine serum (Procell, Wuhan, 164210-50, China) and 1% penicillin-streptomycin (Procell, Wuhan, PB180120, China), while the L-929 cell line was kept in MEM (Procell, Wuhan, PM150410, China) supplemented with 10% fetal bovine serum (Procell, Wuhan, 164210-50, China) and 1% penicillin-streptomycin. Incubation occurred at 37 °C, 5% CO2, and 95% humidity. In cell experiments, we created a 50 mg/mL stock solution by stirring NPs in ultrapure water and sonicating for 2 min (50 kJ). We added it to demethylated medium composed of 10% fetal bovine serum (FBS) and MEM medium. Subsequently, we added varying concentrations of NPs to fresh medium, producing final concentrations of 0, 0.1, 1, and 10 mg/L.

Cell vitality

Cell viability was measured via the CCK-8 method. First, cells were grown in 96-well plates until achieving 70% confluence. Next, TiO_2 NPs were introduced to the cells at concentrations of 0, 0.1, 1, and 10 mg/ml for 24 h. After this, 10 μl of CCK-8 solution (Beyotime, C0037, Jiangsu, China) was carefully added, and the cells were then incubated in a cell incubator for 1–4 h. To measure absorbance at 450 nm, a microplate reader was employed to ascertain four sets of replicate data for each concentration of TiO_2 NPs, and the average value was then calculated.

SiRNA transfection

When the cell density reaches 60–80%, transfected cells should be treated with si-Snai2 and si-Spp1 using GP-transfect-Mate transfection reagent (GenePharma, Shanghai, China). Following this step, TiO_2 NPs should be introduced, and the cells should continue to culture for 24–48 h. The siRNA sequences can be found in the Supplementary Table .

Quantitative Real-Time PCR

Tissue samples were isolated by crushing or washing with PBS before using Trizol reagent (Sigma, St louis, USA) to extract total RNA from both tissue and cell samples. SweScript RT II First Strand cDNA Synthesis Kit (Servicebio, Wuhan, China) was used to synthesize cDNA. Relevant genes, including SPP1, SNAI2, α-SMA, and COL1, were amplified by quantitative polymerase chain reaction (qPCR) using the SYBR green system. The data from RT-qPCR were analyzed using CT and $2^{-\Delta\Delta Ct}$. The qPCR primer sequences used are shown in Table S4.

Western blotting

After extracting proteins from the cells and measuring the protein concentration using a BCA kit, the proteins underwent 4–20% sodium dodecyl sulfate-PAGE electrophoresis (ACE Biotech, Changzhou, China) and were then transferred to polyvinylidene fluoride membranes (Beyotime, Shanghai, China). The details of the antibodies that were used in this research can be found in the supplementary table (Table S2). SNAI2 (CST, 1:1000), α-SMA (CST, 1:1000), SPP1 (Abcam, 1:1000), COL1 (Abcam, 1:1000), PI3K (CST, 1:1000), P-PI3K (CST, 1:1000), AKT (CST, 1:1000), and P-AKT (CST, 1:1000) were subsequently incubated overnight at 4 °C. The secondary antibody utilized in the detection process was horseradish peroxidase-labeled anti-rabbit immunoglobulin and anti-mouse immunoglobulin (BIOSS, Beijing, China) at a 1:5000 dilution. Visualization of protein bands was achieved using a highly sensitive ECL chemiluminescence reagent (NCM Biotech, Suzhou, China), with imaging and photography carried out by an automated chemiluminescence image analysis system (Bio-Rad, Hercules, USA). Grayscale value analysis was then conducted using ImageJ software.

Confocal microscope

C2C12 and L929 cells were cultured in 24-well plates, each with coverslips. The cells were then treated with TiO_2 NPs, and after treatment, they were washed with PBS and fixed with PFA for 15 min. After washing again, the cells were then incubated with 0.1% PBST for 15 min and subsequently blocked with 5% BSA for 1 h. Finally, the cells were incubated overnight at 4 °C with SNAI2 (CST, 1:200), α-SMA (CST, 1:200), SPP1 (Abcam, 1:200), and COL1 (Abcam, 1:200). In the end, a mixture of Actin-Tracker Green-488 and Cy3-conjugated Goat Anti-Rabbit IgG (H+L) was used to incubate the cells

for 1 h. Each well was stained with 200 μL of Solarbio's DAPI solution for 6 min. Subsequently, the images were captured using a Zeiss LSM880(Zeiss, Oberkochen, Germany) and a Leica SP8 confocal microscope (Leica, Wetzlar, Germany).

Cytokine quantification

Enzyme-linked immunosorbent assay kits (Servicebio, Wuhan, China) were utilized for detecting the concentrations of tumor necrosis factor-α, IL-1, and IL-6 in muscle tissue, serum, and cell supernatant. All tests were conducted in accordance with the instructions provided by the manufacturer.

Statistical analysis

The collected data were statistically analyzed using SPSS 25 software (IBM, Chicago, USA). The mean value and standard deviation (SD) of each data point were displayed for statistical analysis. One-way ANOVA and t-tests were performed for comparisons between two or more groups. When the variance was uneven, Dunnet's T3 was utilized, and when the variance was even, LSD was implemented. We considered $P<0.05$ statistically significant. Data were plotted using GraphPad Prism 9.0 software (GraphPad Software, SanDiego, USA).

Results

Tissue fibrosis and muscle damage resulting from metal implant exposure

Titanium alloy is a widely utilized biomaterial in orthopedic surgery due to its excellent biocompatibility. Metal implant exposure can cause tissue fibrosis and muscle damage. We implant titanium and Co-Cr-Mo screws and rods for fixation in spinal surgery (Fig. 1A), and these implants are typically permanent. Interestingly, several years post the initial surgery, a subset of patients who necessitated secondary revision surgery exhibited scar tissue-like hyperplastic lesions and muscle tissue degeneration adjacent to the implants (Fig. 1B). Therefore, we gathered muscle scar tissues surrounding the implants during revision surgery from 8 patients (mean age 31.94±15.40 years) and took tissues from the corresponding area in 8 patients (mean age 35.25±14.55) undergoing initial surgery for H&E, Masson staining, and immunohistochemical analysis (Fig. 1C-E). H&E staining demonstrated that muscle tissues exposed to metal implants displayed disorganization of the myofibrillar structure, reduction of the diameter of the muscle bundles, and hyperplasia of fibrous connective tissue in comparison to the normal controls. Masson staining revealed significant tissue proliferation of collagen fibers in the muscle tissue surrounding the metal implant. Additionally, notable elevation in COL1 expression within the tissue surrounding the metal implant was observed.

The expression of genes associated with fibrosis, specifically Col1 and α-SMA, was examined in further detail. The results indicated a 3.99±0.45 and 1.88±0.12-fold increase in the expression of Col1 and α-SMA, respectively, compared to the control group (Fig. 1F and G). Due to reports of post-surgery pain in some patients, we investigated levels of inflammatory markers IL-6 and TNF-α in the blood of those with implants. The results displayed significant increases, with IL-6 averaging at 20.40 pg/ml and TNF-α at 64.22 pg/ml (Fig. 1H and I). These findings strongly suggest that metal implant exposure induces muscular tissue fibrosis and damage.

Release of titanium nanoparticles from implants and accumulation in surrounding tissues

To determine the cause of fibrosis and muscle damage in tissues surrounding metal implants, we analyzed the elemental composition of the implant removed from the patient (Fig. 2A, B) using SEM-EDS. Spinal metal implants typically consist of titanium and cobalt-chromium-molybdenum (Co-Cr-Mo) alloys. This is in line with the description provided by the manufacturer. SEM analysis revealed defects at the nano-micron level in the surface morphology of the metallic implants (Fig. 2C and D). The Co-Cr-Mo implant was found to be comprised of 65.8% Co and 30.3% Cr (Figure S1C). The chemical composition and surface bonding of titanium implants extracted from patients were analyzed by XPS. The Ti 2p spectra showed characteristic $2p^{3/2}$ and $2p^{1/2}$ peaks of titanium dioxide. Moreover, the presence of O^{2-} states in the implant was confirmed by the binding energy of O 1s photoelectrons (Fig. 2E-G). To confirm the deposition of titanium in the surrounding tissue, we used TEM to scan tissue samples around the implants. The results showed an abundance of nanoscale black particles (Fig. 2H), ranging in size from tens to hundreds of nanometers, consistent with the dimensions of surface defects observed through SEM (Fig. 2C, D). Verification of increased titanium content in proximal tissues of the metal implants was achieved through ICP-MS analysis at varying distances, demonstrating an inverse relationship with distance (Fig. 2I, J). These findings confirm the release of titanium nanoparticles from the implant surface, which then deposit in the surrounding tissues. In subsequent experiments, TiO_2 NPs with particle deposition sizes similar to those observed in tissue TEM were used. SEM showed the aggregation of TiO_2 NPs into nanoscale particles ranging from 62.5 to 500 nm (Figure S2).

Specifically, titanium content was elevated by 159-fold in tissues surrounding the implant (25611±9158 vs. 161±45 μg/kg). We conducted a study to analyze titanium levels in the peripheral blood of patients who received metallic implants. Our findings show that one

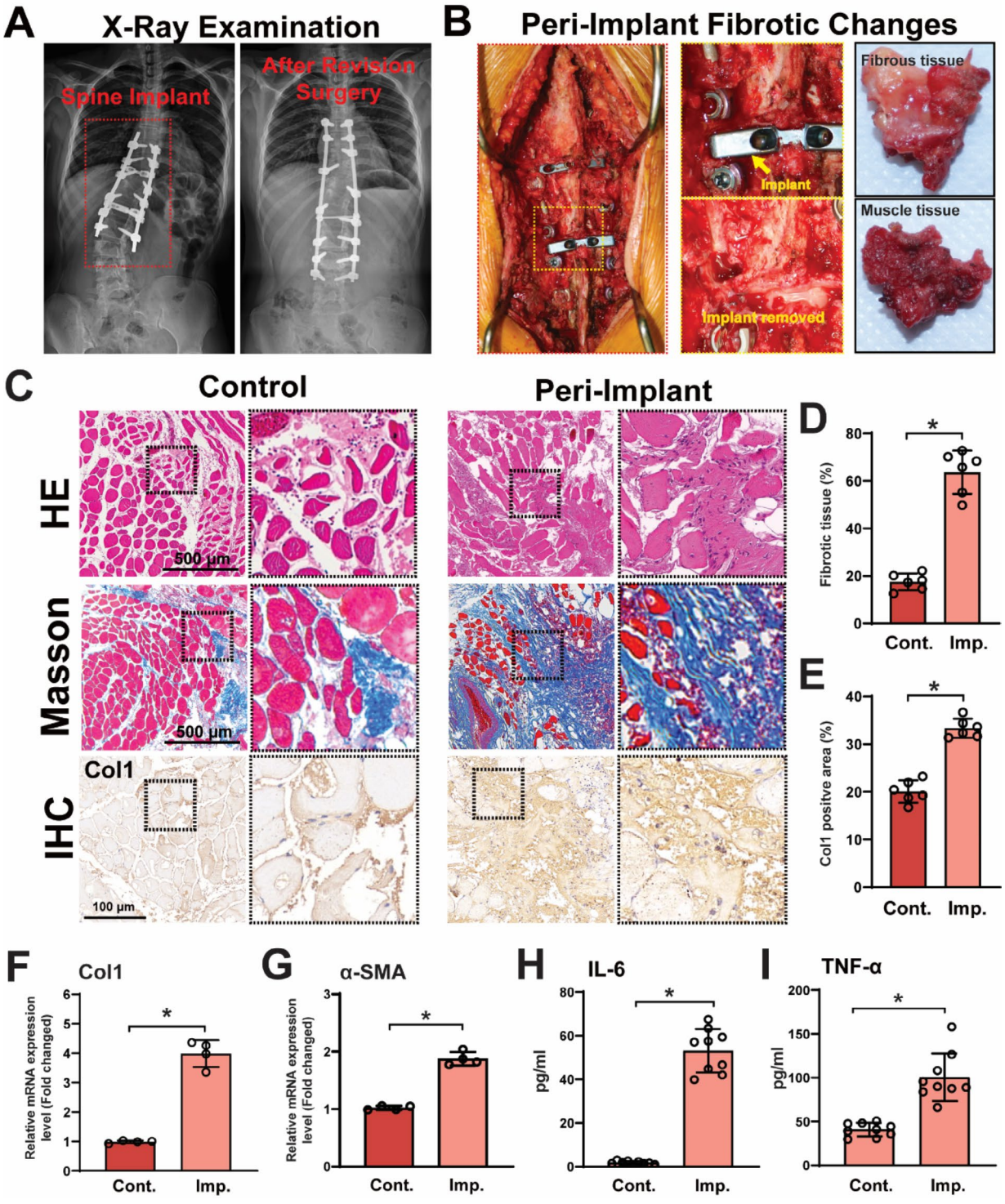

Fig. 1 Exposure of metal implant resulted in tissue fibrosis and muscle injury. (**A**) Titanium screws and Co-Cr-Mo rods were implanted in a patient for fixation during surgery for the correction of scoliosis. The patient underwent a second revision surgery 1 year after the first surgery. Preoperative and post-operative radiographs were obtained. (**B**) At the second surgery, scar tissue-like hyperplastic lesions were seen in the muscle surrounding the implant. (**C**) HE, Masson staining and IHC analysis of tissue around the implant and control. (**D**) Ratio of collagen-stained (blue) to total stained area in Masson staining ($n=6$). (**E**) Semi-quantitative analysis of Col1 signal density in IHC analyses ($n=6$). (**F**, **G**) The mRNA expression of Col1 and αSMA in tissue around implant and control were analyzed by qPCR. The control group was set to 1.0, * means $P<0.05$ between two indicated groups ($n=4$). (**H**, **I**) Blood levels of IL-6 and TNF-α in postoperative patients with low back pain and control were examined by ELISA assay ($n=9$). * means $P<0.05$ between two indicated groups. All data are displayed as mean ± SD

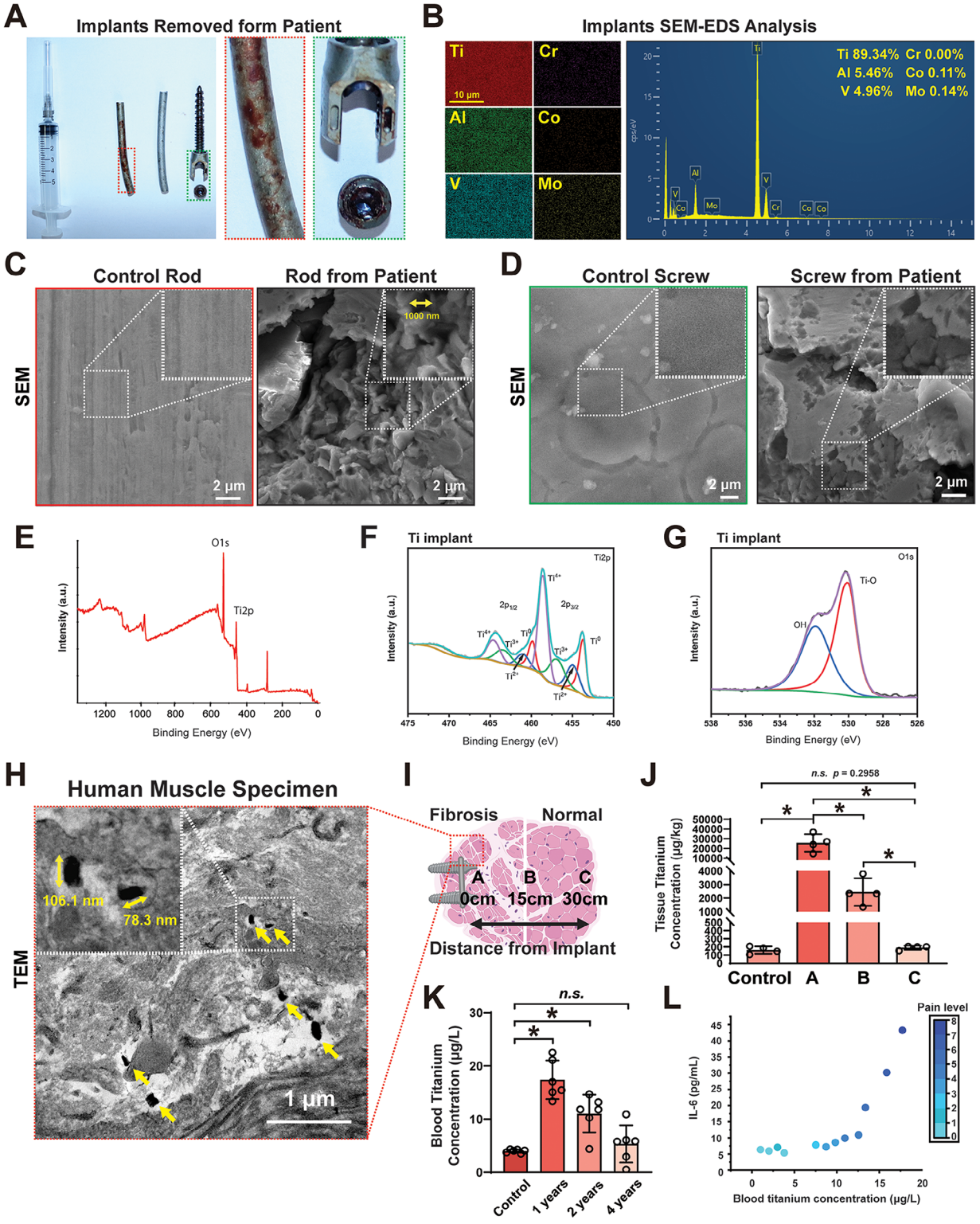

Fig. 2 Sustained release of titanium nanoparticles from implants causing titanium exposure. (**A**) Visualization of implants removed from patients. (**B**) SEM-EDS analysis of Titanium alloy implant removed from patients. (**C**, **D**) SEM analysis of screw and rod removed from patients. (**E**-**G**) Ti 2p, O 1s and Survey XPS spectra of Titanium implant removed from patients. (**H**) Scanning electron micrographs of muscle tissue samples around metal implants. Yellow arrows indicate the black nanoscale metal particles, which vary in size from tens to hundreds of nanometers. (**I**, **J**) Ti content in the tissues at different distances from the implant (0, 15, 30 cm) and control ($n=4$). (**K**) Ti content in the blood of patient at various times after surgery (1, 2 and 4 years) and control ($n=6$). (**L**) Triple Factor Correlation Analysis of blood IL-6 Levels, blood Ti Levels, and Pain Scores in patients with postoperative pain ($n=12$)

year after surgery, titanium content was elevated 4.3-fold (17.42±3.62 vs. 3.99±0.31 μg/L) (Fig. 2K). Although titanium levels in the blood of patients four years after surgery were higher than normal, the difference was not statistically significant (5.33±3.49 vs. 4.00±0.31 μg/L, $p=0.3720$). By analyzing the cobalt and chromium levels in both muscle tissue and blood samples, we observed comparable patterns. However, the increase was less pronounced when compared to titanium (Figure S1 A and B). Therefore, we propose that titanium nanoparticles released from the implant have a significant impact on muscle tissue damage and fibrosis. In addition, we performed a three-way correlation study examining the blood levels of inflammatory factors (IL-6 and TNF-α) and Ti, as well as pain scores, in patients experiencing postoperative pain (Fig. 2L and Figure S3). Our results suggest that the severity of pain experienced by patients increased as blood levels of both IL-6 and Ti (Fig. 2L).

Titanium exposure induces muscle tissue fibrosis in zebrafish and rats

To validate whether titanium plays a role in fibrosis, we used zebrafish and rat models. In the zebrafish model, we exposed zebrafish larvae (2 dpf) to titanium and cobalt nanoparticles in their circulating water (Figure S4A). TiO_2 NPs were detected in zebrafish muscle tissue through TEM imaging (Fig. 3A). Also, titanium levels in both the water and zebrafish exhibited a significant increase, with about 75,900-fold increase observed in zebrafish muscle tissue (0.020±0.009 vs. 1518.308±621.504 μg/kg) (Fig. 3B). This suggests that TiO_2 NPs can penetrate zebrafish muscle tissue through water. The survival rate of zebrafish decreased as the concentration of nanoparticles increased, although there was no significant difference in the hatching rate (Fig. 3C, Figure S4B-D). After 4 days of treatment, the zebrafish subjected to 80 mg/L of TiO_2 NPs had a survival rate of 31%, which was lower compared to those exposed to cobalt nanoparticles (Fig. 3C and Figure S4C, D). We collected zebrafish tissue after seven days of treatment. The muscle tissues that contained TiO_2 NPs exhibited disorganization in the myotome structure (Fig. 3A). H&E staining revealed TiO_2 NPs exposure caused disorganization of myotome structure and reduced muscle bundles compared to the control group (Fig. 3D). Masson staining suggested the proliferation of fibrous tissues rich in collagen within TiO_2 NPs-exposed zebrafish muscle tissue samples (Fig. 3E).

Subsequently, a rat titanium implant model was established (Fig. 3F). Titanium implants were sectioned into small pieces and implanted into subcutaneous muscle tissues on the dorsum of rats (Figure S5A). After 30 days, the respective tissue samples were collected. A slight hyperplasia of scar tissue was observed surrounding the implant (Fig. 3G) and the ICP-MS analysis indicated the accumulation of titanium in the tissue adjacent to the implant (Figure S5B, Table S3). Consistent with our observations in humans, we found that the levels of COL1 expression were markedly upregulated in the peri-implant area (Fig. 3H and L). In addition, H&E and Masson stainings revealed abnormal myofibrillar structure, hyperplasia of fibrous connective tissue and significant collagen deposition in the muscle tissue of rats exposed to titanium implants (Fig. 3I, J and M), consistent with previous studies [23]. In addition, there was an increase in the expression of Col1 and α-SMA in the muscle tissues (Fig. 3K and N, Figure S5C) of rats exposed to titanium implants. These results suggest that both TiO_2 NPs and titanium implants may result in muscle tissue fibrosis.

TiO_2 NPs exacerbate in vitro muscle injury and fibrosis

We developed a cellular model using TiO_2 NPs (Fig. 4A) by administered 0, 0.1, 1, and 10 μg/mL TiO_2 NPs to L929 and C2C12 cells, respectively. TiO_2 NPs entered the cytoplasm and nucleus of L929 and C2C12 cells, as observed by TEM (Fig. 4B). Confocal microscopy also showed that FITC-labeled TiO_2 NPs [24] entered the cells and were distributed in both the cytoplasm and nucleus (Figure S6A, B). Interestingly, exposure to 0.1 μg/mL of TiO_2 NPs for 24 h resulted in a slight increase in the viability of L929 and C2C12 cells. However, when exposed to 10 μg/mL of TiO_2 NPs, the viability of L929 and C2C12 cells decreased to 80.5% and 77.9%, respectively (Fig. 4C), which is consistent with a previous study [25]. Furthermore, exposure of L929 cells to 0.1 μg/mL TiO_2 NPs resulted in increased mRNA expression of COL1 (2.54-fold) and α-SMA (1.94-fold), whereas exposure to 10 μg/mL TiO_2 NPs resulted in a significant decrease in the expression of COL1 and α-SMA, possibly due to cytotoxicity caused by the increase in concentration (Fig. 4D, E). Similar results were observed in the C2C12 cell line (Figure S6C). Protein quantification confirmed the findings at the RNA level, showing that COL1 and α-SMA protein expression increased by 2.93±0.29 and 2.29±0.05-fold, respectively, after the addition of 0.1 μg/mL TiO_2 NPs to the culture medium for 48 h (Fig. 4F, G). In addition, our observations showed a significant increase in the intracellular expression of COL1 and α-SMA in L929 and C2C12 cells after exposure to TiO_2 NPs (Fig. 4H-L). These findings strongly indicate that exposure to TiO_2 NPs in vitro upregulates the expression of genes related to fibrosis. Interestingly, by co-culturing L929 and C2C12, we found that exposure to TiO_2 NPs resulted in increased levels of inflammatory markers IL-6 and TNF-α compared to culture individually (Fig. 4M, N). This indicates that the two types of cells work together to intensify the inflammatory response when treated with TiO_2 NPs.

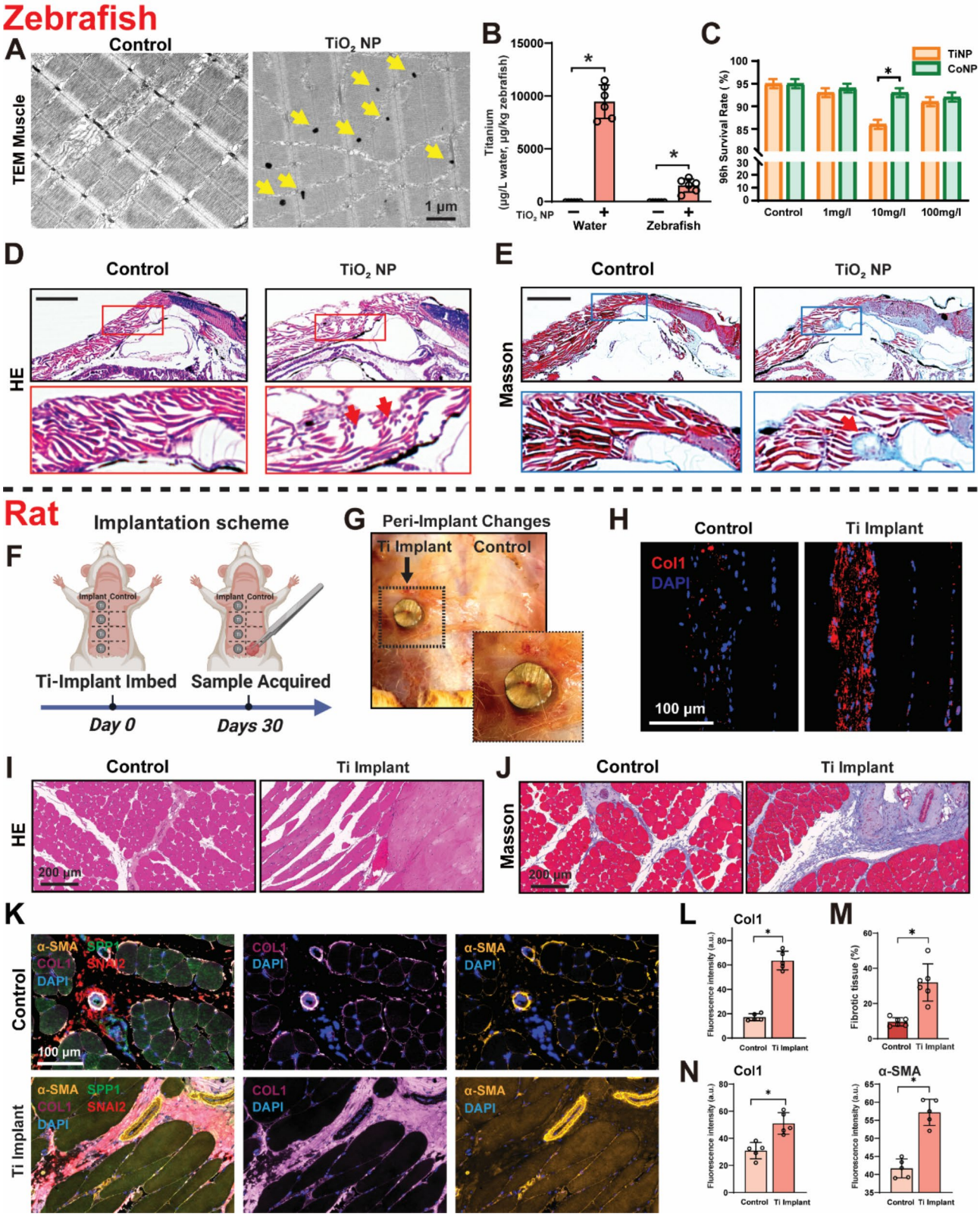

Fig. 3 (See legend on next page.)

(See figure on previous page.)

Fig. 3 Titanium exposure results in muscle fibrosis in zebrafish and rats. (**A**) TiO_2 NPs treated zebrafish were observed using TEM after 7 days treatment. The muscle tissue was extracted and analyzed. Yellow arrows indicated the TiO_2 NPs entering muscle tissue. (**B**) Ti content in the water and zebrafish muscle treated with TiO_2 NPs and control ($n=6$). (**C**) Zebrafish embryos survival proportions treated with 1-100 mg/L TiO_2 NPs for 24 h. (**D**, **E**) HE, Masson staining of zebrafish treated with TiO_2 NPs for 7days. Scale bar = 1 mm. (**F**) Schematic illustrates the rat experimental design. (**G**) One-month post-implantation view of a titanium alloy implanted in the dorsal subcutaneous muscle of rat. Right side tissue was used as self-control. (**H**) IHC analysis of Col1 and αSMA for muscle tissue after titanium alloy implantation and control. (**I**, **J**) HE, Masson staining of rat dorsal subcutaneous muscle implanted with Ti alloy for 30 days. (**K**) Immunofluorescence staining of muscle tissues around Ti implant for collagen I (purple), α-SMA (yellow), SNAI2 (red) and SPP1 (green), counterstained with DAPI (blue) for cell nuclei. (**L**) Quantification for signal density in muscle tissue around implant and control for Col1 (H) ($n=5$). (**M**) Ratio of collagen-stained (blue) to total stained area in Masson staining (**J**) ($n=6$). (**N**) Quantification for signal density in muscle tissue around implant and control for Col1 and α-SMA ($n=5$). * means $P<0.05$ between two indicated groups. All data are displayed as mean ± SD

TiO_2NPs regulate muscle tissue fibrosis via activation of the SNAI2-SPP1-PI3K/AKT Axis

To investigate the molecular mechanism of TiO_2 NPs leading to fibrosis, we conducted transcriptomic analysis of human muscle tissues. RNA sequencing was performed on muscle tissue samples collected during surgery from four implanted muscles and four healthy control muscles. Differentially Expressed Genes (DEGs) and Kyoto Encyclopedia of Genes and Genomes (KEGG) pathway enrichment analysis revealed a remarkable enrichment of the PI3K/AKT pathway, indicating that its potential may be significant in this process (Fig. 5A). A subset of DEGs and KEGGs were associated with fibrosis-related genes, and heat map analysis (Fig. 5B) showed that the expression of fibrosis-related genes, specifically Snai2, was significantly upregulated compared to the control group, as confirmed by protein expression at the tissue level (Fig. 5C and D). To further validate this finding, we collected rat muscle tissues and conducted qPCR analysis on multiple fibrosis-related genes. Upon analyzing the clustered heatmap of fibrotic gene expression levels, it revealed that fibrotic gene expression significantly increased in muscle tissues adjacent to titanium implants. Specifically, the expression of Snai2 was notably higher compared to the control group (Fig. 5E), also confirmed by elevated protein expression (Fig. 5F). Additionally, the expression regions of Snai2 and Col1 strongly overlapped, indicating a potential regulatory relationship (Fig. 5F).

To further elucidate the role of Snai2 in TiO_2 NPs-induced fibrosis, we administered 0.1 μg/mL TiO_2 NPs to a cell model after L929 cell treatment. We observed a significant increase in Snai2 nucleus expression (Fig. 5G, H). Although silencing Snai2 expression did not show any significant difference in Col1 expression, the impact of TiO_2 NPs in promoting Col1 expression was meaningfully curtailed (Fig. 5I, J). After suppressing Snai2 expression, TiO_2 NPs were unable to induce COL1 and α-SMA expression in muscle tissue (Fig. 5K, L). These results suggest that TiO_2 NPs stimulate the expression of Snai2 and consequently promote fibrosis formation.

We examined the downstream molecular pathways of Snai2. Analysis of the RNA-seq enrichment results showed that the expression of SPP1 is significantly upregulated (Fig. 6A and B). Furthermore, an enhanced increase in Spp1 expression was confirmed in cell lines after TiO_2 NPs treatment (Fig. 6C, D). Protein expression results indicate a reduction in Spp1 expression following the silencing of Snai2 expression. However, there was no significant alteration in Snai2 expression after Spp1 silencing (Fig. 6E, F). Moreover, TiO_2 NPs led to an increase in intracellular co-expression of Snai2 and Spp1. Snai2 signals were mainly concentrated in the nucleus and silencing Snai2 led to reduced levels of both Snai2 and Spp1 expression. However, the silencing of Spp1 did not affect Snai2 expression. These findings suggest that Snai2 may function as an upstream transcription factor of Spp1. Upon silencing the expression of Spp1, the elevated expression of Col1 induced by TiO_2 NPs was suppressed (Fig. 6H, I). Therefore, Snai2 appears to regulate fibrosis via modulation of Spp1 expression upon activation by TiO_2 NPs. Furthermore, PI3K pathway activation was examined after TiNP exposure. Significant increases in p-PI3K and p-AKT levels were observed, indicating stimulation of the PI3K/AKT pathway. Furthermore, the silencing of Snai2 suppressed the degree of activation of the PI3K/AKT pathway (Fig. 6J, K), suggesting that TiO_2 NPs regulate cellular fibrosis via activation of the SNAI2-SPP1-PI3K/AKT axis.

Snai2 knockdown inhibits titanium implant-induced fibrosis in vivo

In order to further validate the therapeutic targeting role of Snai2 in fibrosis caused by titanium nanoparticle exposure, we conducted in vivo model rescue experiments. By utilizing Cas9 knockout strategy, we constructed a zebrafish model of *snai2*$^{-/-}$. TiO_2 NPs were administered at 2 dpf and morphological changes were evaluated at 5 dpf. Tissue samples were collected from zebrafish at 9 dpf (Figure S7A). Through qPCR analysis of the zebrafish tissue samples, it was observed that the expression of *snai2* decreased, indicating the successful modeling of *snai2* knockout zebrafish (Figure S7B). In addition, the promotion of *spp1* and *col1a1a* by TiO_2 NPs treatment was impeded by the knockout of *snai2* (Fig. 7B, C). The results of HE and Masson stainings demonstrated that TiO_2 NPs -exposed *snai2*$^{-/-}$ zebrafish exhibited a notable

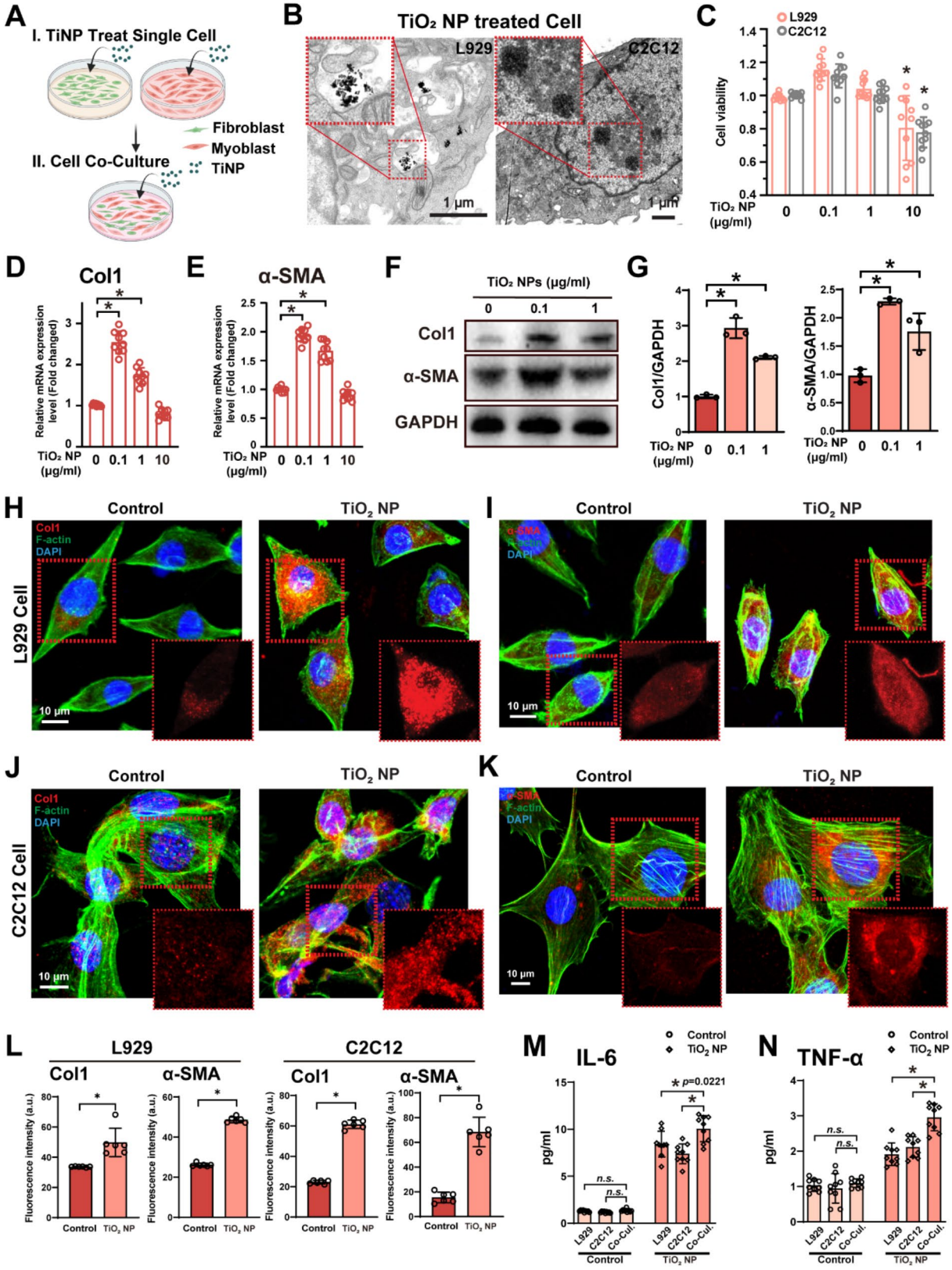

Fig. 4 (See legend on next page.)

(See figure on previous page.)

Fig. 4 TiO_2 NPs exposure activated the fibroblasts and myoblasts. (**A**) Schematic illustrates the cell experimental design. (**B**) TEM of cells treated with TiO_2 NPs. Red boxes showed nanoparticle aggregates in cell plasma and nucleus. (**C**) Cell viability of L929 and C2C12 cells treated with 0.1–10 μg/ml TiO_2 NPs for 24 h. *$P < 0.05$ versus 0 group. (**D**, **E**) The mRNA expression of Col1 and αSMA in L929 cells treated with 0.1–10 μg/ml TiO_2 NPs and control were analyzed by qPCR. The control group was set to 1.0, * means $P < 0.05$ between two indicated groups ($n = 9$). (**F**) The expression of Col1 and αSMA in cells treated with 0.1–1 μg/ml TiO_2 NPs and control were analyzed by Western blotting. GAPDH was used as internal reference. (**G**) Relative expression levels were compared between the TiO_2 NPs-treated cells and the control cells. (**H**-**K**) Immunofluorescence staining of cells treated with 0.1 μg/ml TiO_2 NPs and control for Col1 (red), α-SMA (red) and F-actin (green), counterstained with DAPI (blue) for cell nuclei. (**L**) Quantification for signal density in cells treated with 0.1 μg/ml TiO_2 NPs and control for Col1 and α-SMA ($n = 6$). (**M**, **N**) IL-6 and TNF-α levels in culture medium of cells treated with 0.1 μg/ml TiO_2 NPs and blank control were examined by ELISA assay ($n = 9$). * means $P < 0.05$ between two indicated groups. All data are displayed as mean ± SD

decrease in muscle tissue fibrosis and damage as compared to TiO_2 NPs-exposed wild-type zebrafish (Fig. 7D, E).

In the rat model, we silenced snai2 in subcutaneous tissues using a gel wrapped with snai2 siRNA. Then, we administered siRNA around the titanium implants on days 3, 12, and 21 after modeling (Fig. 7F). The protein expression assay indicated effective silencing of Snai2 expression (Fig. 7G, K). Silencing the expression of Snai2 effectively prevented alterations to rat muscle tissues resulting from damage caused by TiO_2 NPs, which involved changes in muscle fascicle arrangement patterns, increased muscle fascicle density, reduced connective tissue envelope, and proliferation of fibrous tissue (Fig. 7H, I, and L). Immunofluorescence results in rat muscle tissue exhibited that Snai2 silencing reduced fibrosis and significantly decreased the expression of Col1 and α-SMA induced by Ti implant (Fig. 7J and M). These outcomes indicate the significant role of snai2 in the development of fibrosis due to Ti exposure.

Discussion

The rapid development of biomaterials technology has led to the widespread use of titanium implants in the biomedical field, effectively addressing clinical problems in orthopedics and dentistry. However, it is important to note that once implanted in the human body, these titanium implants can remain present for decades or even a lifetime. The human body typically contains very little titanium, and any accumulation of this element in the body is usually due to long-term occupational exposure or release from titanium implants. Titanium implants are generally considered inert and biocompatible [2]. Recent clinical evidence suggests that long-term implantation of titanium implants may release tiny metal particles or ions due to wear or corrosion. These particles or ions may be deposited into surrounding tissues and migrate to distant sites, potentially affecting the tissues surrounding the implant and distant organs [26]. Titanium implants may have adverse effects on distant organs, such as nerve tissue in the brain, or on the cardiovascular system [8]. Complications may include neuropathy [17] or thrombosis [27]. In addition, the presence of titanium particles around joint prostheses may inhibit osteogenesis [28]. Research has shown that metal nanoparticles can have toxic effects on skeletal muscle tissue [29], therefore further investigation is needed into the specific effects of titanium nanoparticles on the connective tissue of the muscle surrounding the implant due to long-term exposure to titanium implants.

After being implanted in the human body, titanium implants continuously release titanium particles for an extended period. As these implants wear and corrode, they release potentially harmful metal particles into adjacent or distant tissues and organs. We have, for the first time, directly observed nanoparticles in the tissues surrounding the implant. Moreover, there is a noteworthy rise in titanium content in the proximity of the implant. SEM revealed nanoscale defects on the surface of the titanium alloy implant. These results confirm the release of nanoscale titanium particles from the implant surface into the surrounding tissue. XPS analysis showed that the main component on the surface of the extracted implant from the human body was TiO_2, the most common natural oxide of titanium. Therefore, we utilized TiO_2 NPs to establish an experimental model of titanium exposure to investigate the mechanisms by which nanoscale titanium particles induce fibrosis.

TiO_2 NPs exposure significantly increased the risk of muscle damage and fibrosis. In rats, Intravenous injection of TiNPs resulted in muscle inflammation and atrophy [30]. Furthermore, chronic exposure to TiO_2 NPs over the long-term activated myocardial fibrosis in rats [15, 31]. Muscle tissue fibrosis usually entails structural damage, faulty regeneration, excessive collagen accumulation, and ECM generation [31]. To confirm the hypothesis that TiO_2 NPs provoke muscle tissue injury and fibrosis, we created a TiO_2 NPs-treated zebrafish model and a titanium implant-treated rat model. Zebrafish that received treatment with TiO_2 NPs demonstrated a decrease in muscle bundles and an increase in fibrosis. Similarly, in the rat model with titanium implants, we observed collagen accumulation and muscle tissue damage. The proliferation and differentiation of fibroblasts and myofibroblasts are significant factors contributing to muscle tissue fibrosis, with α-SMA serving as a crucial marker of myofibroblasts [32]. In the present study, α-SMA and COL1 expression were significantly upregulated in titanium implant-treated rat muscle tissues and TiO_2 NPs-treated C2C12 and L929 cells. This indicates

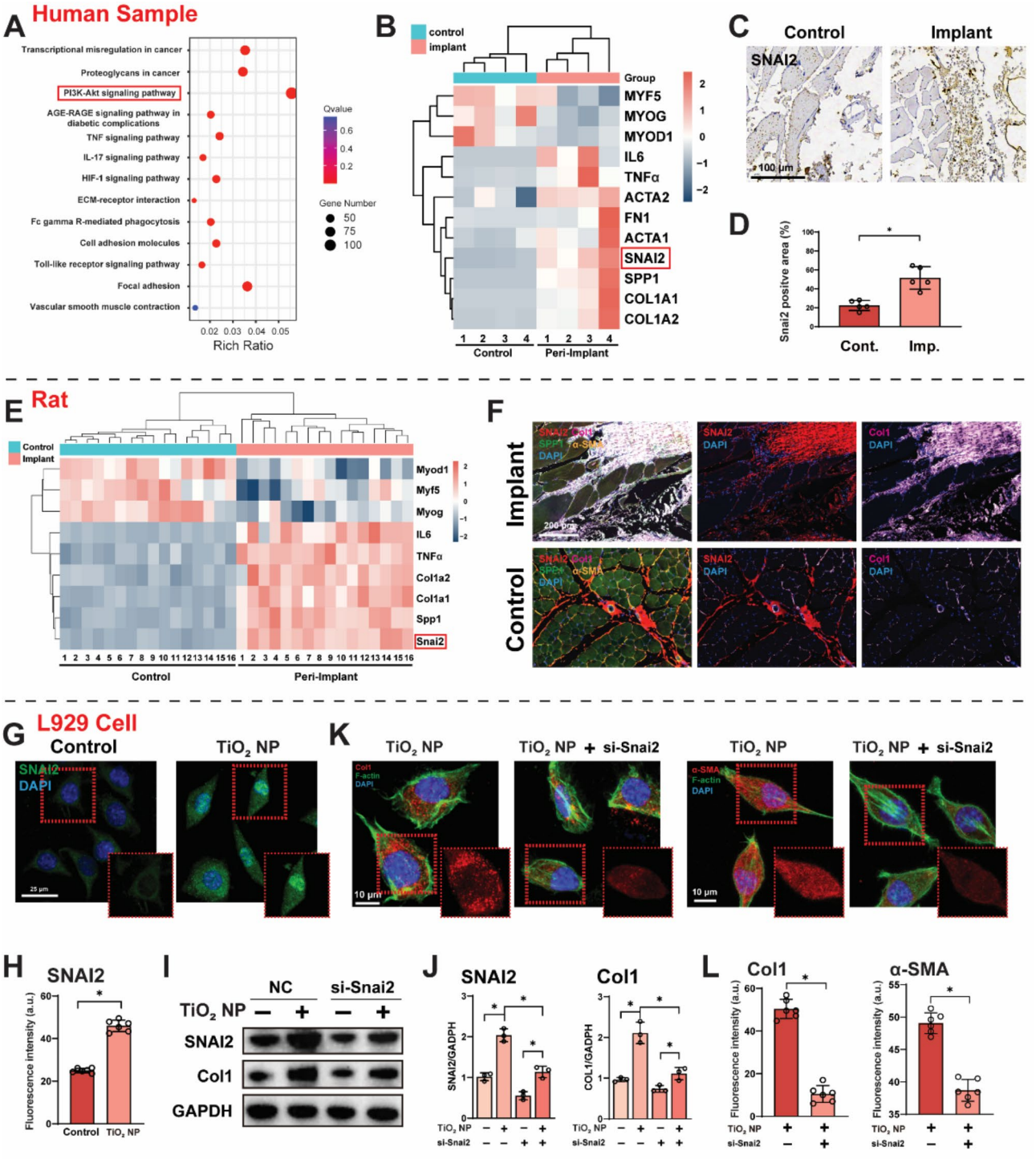

Fig. 5 (See legend on next page.)

(See figure on previous page.)

Fig. 5 TiO_2 NPs up-regulates SNAI2 to activate the expression of fibrosis-associated genes. (**A**) KEGG pathway enrichment analysis of differentially expressed genes between muscle tissue surrounding the implant and control. RNA-seq data was obtained from four muscle tissues around implant and four controls, the muscle tissues were harvested during surgery. (**B**) Heatmap of 12 fibrosis-related genes enriched from DEGs and KEGG pathway enrichment analysis. (**C**) IHC analysis of SNAI2 for muscle tissue around implant and control. (**D**) Semi-quantitative analysis of SNAI2 signal density in IHC analyses (**C**) ($n=5$). (**E**) Heatmap of nine fibrosis-related genes identified in RNA-seq, mRNA expression data was obtained in muscle samples from rat implanted with Ti alloy and sham surgery control ($n=16$). (**F**) Immunofluorescence staining of rat muscle tissues around Ti implant, for collagen I (purple), α-SMA (yellow), SNAI2 (red) and SPP1 (green), counterstained with DAPI (blue) for cell nuclei. (**G**) Immunofluorescence staining of cells treated with 0.1 μg/ml TiO_2 NPs and control for SNAI2 (green), counterstained with DAPI (blue) for cell nuclei. (**H**) Quantification for signal density in immunofluorescence staining of cells (G) for SNAI2 ($n=6$). (**I**) The L929 cells were treated with combination of 0.1 μg/ml TiO_2 NPs treatment and Snai2 siRNA transfection, expression of COL1 and SNAI2 were analyzed by Western blotting. GAPDH was used as internal reference. (**J**) Relative expression levels, normalized to the internal reference protein, were compared between the different treated cells. (**K**) The L929 cells were transfected with Snai2 siRNA 6 h before 0.1 μg/ml TiO_2 NPs treatment. Immunofluorescence staining for Col1 and α-SMA (green), counterstained with DAPI (blue) for cell nuclei was performed. (**L**) Quantification for signal density in immunofluorescence staining (**K**) for Col1 and α-SMA was calculated and compared. * means $P<0.05$ between two indicated groups. All data are displayed as mean ± SD

the formation of myofibroblasts and the initiation of the fibrotic process. Additionally, IL-6 and TNF-α exhibited up-regulation in human samples, animal tissue samples, and cell supernatants compared to controls and are commonly used markers of muscle tissue damage [33]. These findings indicate that exposure to titanium nanoparticles may result in significant muscle fibrosis.

TiO_2 NPs have the potential to affect cells and tissues through a variety of pathways and thereby induce fibrosis. These nanoparticles are capable of inducing oxidative stress [34], which causes the production of significant quantities of reactive oxidizing substances (ROS). ROS disrupts the intracellular environment, inciting an inflammatory response that results in tissue cell injury. Additionally, the body's inflammatory response activates inflammatory cells, including macrophages, which release inflammatory mediators, causing muscle tissue injury and contributing to the fibrotic process [35]. It has been suggested that TiO_2 NPs can activate matrix metalloproteinases (MMPs), resulting in collagen breakdown and formation of muscle tissue scarring and fibrosis [36]. TiO_2 NPs may also be involved in muscle fibrosis development through the aberrant activation of the TGF-β/Smad pathway [20]. Abnormal activation of the NF-κB pathway, induced by exposure to TiO_2 NPs, may result in elevated collagen synthesis and reduced protein degradation. This process can contribute to fibrosis progression [31].

In our research, PI3K/AKT pathway was enriched, and high expression of SNAI2 and SPP1 were confirmed. Previous research has suggested a possible link between SPP1 overexpression and fibrogenesis via regulation of inflammatory responses [37]. SPP1 is thought to play an important role in fibrogenesis by activating the PI3K/Akt pathway, which in turn regulates cell proliferation, differentiation, and matrix synthesis. In addition, and for the first time, we found that TiO_2 NPs may promote the expression of SNAI2. SNAI2 accelerates collagen deposition at the site of fibrosis by regulating the expression of extracellular matrix-related genes and promoting the atypical synthesis of collagen and other matrix molecules [38]. Previous research has shown that SNAI2 acts upstream of SPP1, consistent with what we found [39]. To further investigate the effect of SNAI2 after TiO_2 NPs exposure, we suppressed the expression of SNAI2 and observed a reversal of both fibrotic and inflammatory damage induced by TiO_2 NPs. Therefore, the SNAI2-SPP1-PI3K/AKT pathway may serve as an effective therapeutic approach to mitigate muscle tissue damage and fibrosis induced by TiO_2 NPs exposure.

Previous studies have shown that the extracellular matrix plays a critical role in fibrosis, and Snai2 may play a key role in its remodeling process. Snai2 has been reported to play an important role in liver fibrosis (associated with non-alcoholic fatty liver disease) [40], renal interstitial fibrosis (RIF) [41], and hypertrophy of the ligamentum flavum [42]. Combining our results, we therefore sought to determine whether inhibition of Snai2 expression in vivo could alleviate fibrosis caused by TiO_2 NPs/titanium implant. In the zebrafish model, we constructed a *snai2*$^{-/-}$ zebrafish model and found that knockout of the *snai2* gene could inhibit muscle damage and fibrosis induced by TiO_2 NPs. In addition, in the rat received titanium implant model, we observed a significant reduction in the degree of fibrosis caused by local inhibition of snai2 expression. The above results suggest that inhibition of Snai2 expression has therapeutic effects on titanium exposure-induced fibrosis, providing support for potential therapeutic targets. In the future, the development of drugs or other treatments that intervene in Snai2 expression may provide new avenues for alleviating fibrotic diseases associated with titanium implants. In addition, to further mitigate the side effects of particles originating from implants, surface modification techniques, such as coating or surface passivation, could be employed [43, 44]. Additionally, developing novel nanoparticle immobilization techniques is an essential strategy to prevent adverse effects. For instance, utilizing chemical bonding or physical adsorption methods can securely anchor nanoparticles to the titanium alloy surface, thereby minimizing particle detachment and release [45, 46].

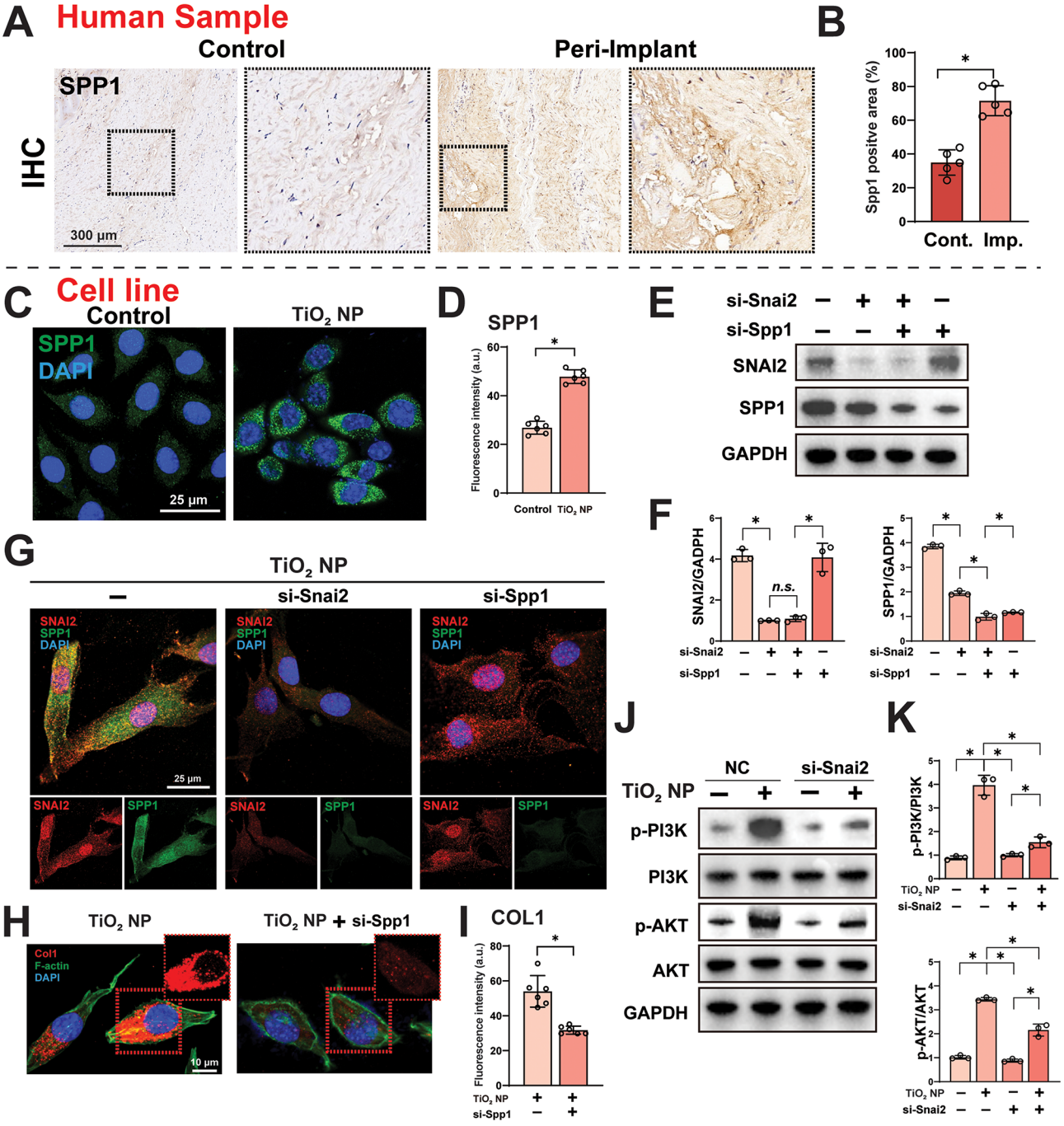

Fig. 6 The profibrogenic effect of SNAI2 was mediated by SPP1 and PI3K pathway. (**A**) IHC analysis of SPP1 for muscle tissue sample around implant and control sample from first surgery patient. (**B**) Semi-quantitative analysis of SPP1 signal density in IHC analyses (**A**) ($n=5$). (**C**) Immunofluorescence staining of cells treated with 0.1 μg/ml TiO_2 NPs and blank control for SPP1 (green), counterstained with DAPI (blue) for cell nuclei. (**D**) Quantification for signal density in immunofluorescence staining of cells (**C**) for SPP1 ($n=6$). (**E**) The L929 cells were treated with combination of Spp1 and Snai2 siRNA transfection under 0.1 μg/ml TiO_2 NPs treatment, expression of SNAI2 and SPP1 were analyzed by Western blotting. GAPDH was used as internal reference. (**F**) Relative expression levels, normalized to the internal reference protein, were compared between the different treated groups. (**G**) The L929 cells were treated with Spp1 or Snai2 siRNA transfection under 0.1 μg/ml TiO_2 NPs treatment, intracellular expression of SNAI2 (red) and SPP1 (green) were detected by immunofluorescence staining, nuclei were stained with DAPI (blue). (**H**) Immunofluorescence staining of cells treated with Spp1 siRNA transfection under 0.1 μg/ml TiO_2 NPs treatment for Col1 (red) and F-actin (green), counterstained with DAPI (blue) for cell nuclei. (**I**) Quantification for signal density of Col1 in staining (**H**) ($n=6$). (**J**) The L929 cells were treated with combination of 0.1 μg/ml TiO_2 NPs treatment and Snai2 siRNA transfection, expression of PI3K, p-PI3K, AKT and p-AKT were analyzed by Western blotting. GAPDH was used as internal reference. (K) Relative expression levels, normalized to the internal reference protein, were compared between the different treated cells (**J**) ($n=3$). * means $P<0.05$ between two indicated groups. All data are displayed as mean ± SD

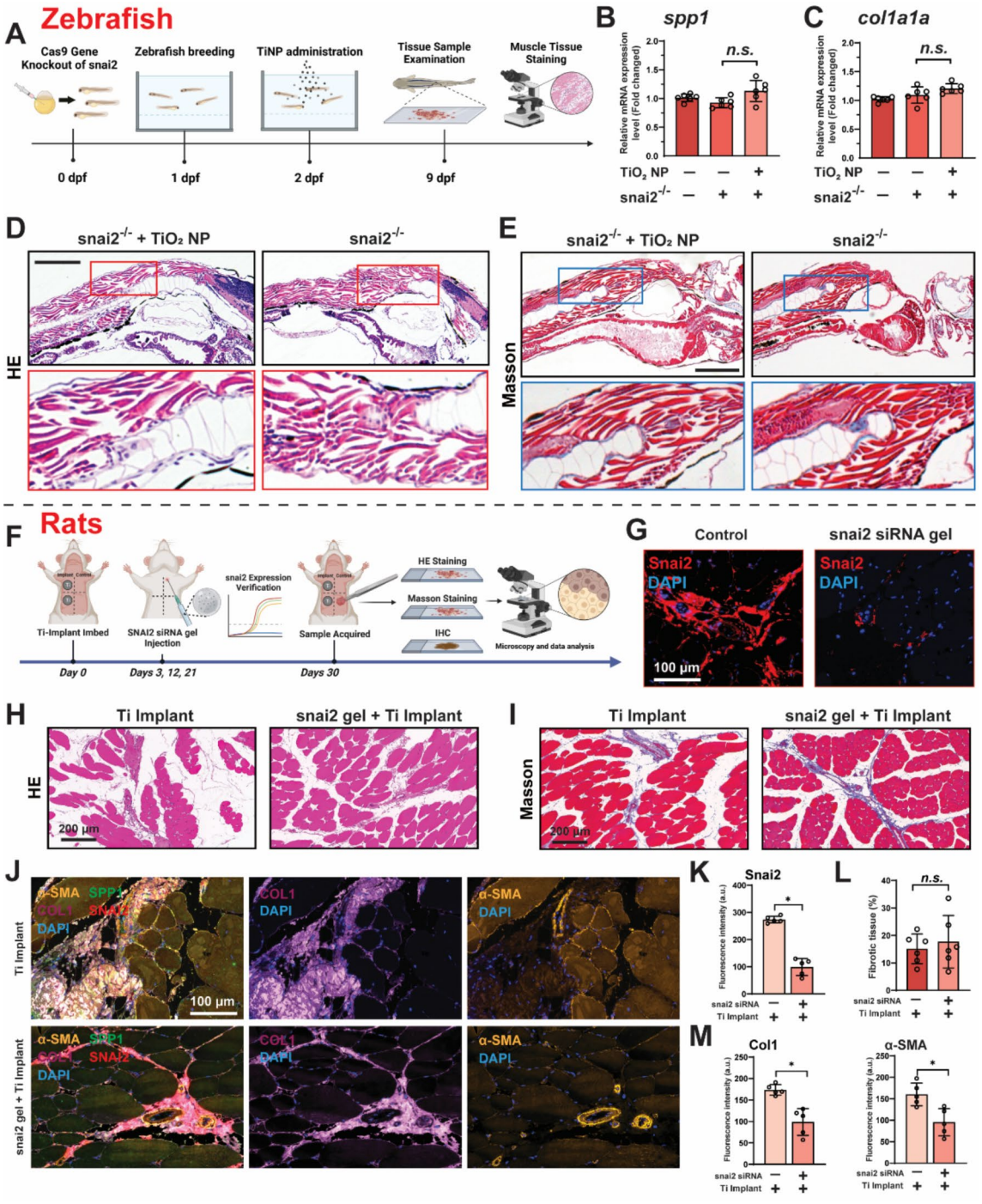

Fig. 7 Knockdown of Snai2 inhibits titanium implant-induced fibrosis in vivo. (**A**) Schematic illustrates the zebrafish experimental design. (**B**, **C**) The mRNA expression of *spp1* and *col1a1a* in wildtype and *snai2*$^{-/-}$ zebrafish larvae treated with TiO_2 NPs were determined by qPCR. Wildtype was set to 1.0 as control group ($n=6$). (**D**, **E**) HE, Masson staining of *snai2*$^{-/-}$ zebrafish larvae treated with TiO_2 NPs for 7days. Scale bar = 1 mm. (**F**) Schematic illustrates the rat experimental design. (**G**) Immunofluorescence detection of Snai2 (red) expression in rat dorsal subcutaneous muscle after siRNA gel treatment, nuclei were stained with DAPI (blue). (**H**, **I**) HE, Masson staining of rat dorsal subcutaneous muscle implanted with Ti alloy implant treated with siRNA gel for 30 days. (**J**) Immunofluorescence staining of rat muscle tissues around Ti implant for collagen I (purple), α-SMA (yellow), SNAI2 (red) and SPP1 (green), counterstained with DAPI (blue) for cell nuclei. (**K**) Quantification for signal density in immunofluorescence staining of rat muscle cross-section (**G**) for Snai2 ($n=6$). (**L**) Ratio of collagen-stained (blue) to total stained area in Masson staining (**I**) ($n=6$). (**M**) Quantification for signal density in muscle cross-section (**J**) for Col1 and α-SMA ($n=5$). * means $P<0.05$ between two indicated groups. All data are displayed as mean ± SD

The quantity of nanoparticles released from titanium implants may be influenced by a multitude of factors, including the implantation site, the immune microenvironment surrounding the implant, and the physicochemical properties of the implant itself. Additionally, the shape of the implant and the size of the surface area may also impact the release. Consequently, when designing the next generation of implant, it is essential to consider these factors to enhance the implant design. Metal particles released from the implant can enter the bloodstream and cause excessive metal levels [47]. In an analysis of postoperative patient blood samples, blood titanium levels were found to correlate with the degree of implant wear [48]. Some spinal implants may release Titanium, Neodymium, and Vanadium, leading to metal-related diseases [9]. Our research suggests that elevated blood titanium levels may serve as a biomarker for inflammation. Patients with postoperative pain had elevated serum levels of inflammatory factors, with a threefold correlation between IL-6 levels, titanium levels, and patient pain scores. This study also has several limitations. Because of the difficulty in obtaining the necessary tissue samples for this study, more clinical data are needed on the way of titanium accumulation around implants. The toxicity of nanoparticles released from titanium implant wear is related to factors such as shape, surface area, and size. Although we selected TiO_2 NPs of similar size, there is still a gap in the representation of titanium nanoparticles released in vivo. In addition, we did not investigate the effect of titanium implants on other organs, which needs to be further investigated.

Conclusions

Our results showed that titanium nanoparticles released from titanium implants may have caused fibrosis in the surrounding tissue. The potential mechanism of fibrosis mediated by the SNAI2-SPP1-PI3K/AKT axis. Upon contact, titanium nanoparticles penetrate relevant tissues and cells, activating SNAI2 expression. This in turn modulates downstream signaling pathways, including SPP1 and PI3K/AKT, ultimately resulting in fibrosis and inflammatory injury. Our findings provide new insights into the source of titanium nanoparticles from metallic implants, their potential toxicity, and the mechanism by which they affect surrounding tissues.

Supplementary Information

The online version contains supplementary material available at https://doi.org/10.1186/s12951-024-02762-4.

Supplementary Material 1

Supplementary Material 2

Acknowledgements
Some of the images included in the article were sourced from biorender.com, for which we are grateful.

Author contributions
Gengming Zhang: Investigation, Software, Validation. Linhua Deng: Conceptualization, Formal analysis, Software, Investigation, Validation, Visualization, Writing – original draft. Zhongjing Jiang: Methodology, Resources. Gang Xiang: Investigation, Resources. Zhuotong Zeng: Conceptualization, Resources. Hongqi Zhang: Funding acquisition. Yunjia Wang: Investigation, Conceptualization, Data curation, Funding acquisition, Project administration, Software, Supervision, Visualization, Writing – original draft, Writing – review & editing.

Data availability
No datasets were generated or analysed during the current study.

Declarations

Competing interest
The authors declare no competing interests.

Author details
[1]Department of Spine Surgery and Orthopaedics, Xiangya Hospital, Central South University, Changsha, Hunan 410008, China
[2]National Clinical Research Center for Geriatric Disorders, Xiangya Hospital, Central South University, Changsha, Hunan 410008, China
[3]College of Environmental Science and Engineering, Key Laboratory of Environmental Biology and Pollution Control (Hunan University), Hunan University, Ministry of Education, Changsha 410082, PR China
[4]Department of Dermatology, Second Xiangya Hospital, Central South University, Changsha 410011, PR China

Received: 13 May 2024 / Accepted: 9 August 2024
Published online: 30 August 2024

References

1. Sidambe AT. Biocompatibility of Advanced Manufactured Titanium Implants-A Review. Mater (Basel). 2014;7:8168–88.
2. Kaur M, Singh K. Review on titanium and titanium based alloys as biomaterials for orthopaedic applications. Mater Sci Eng C Mater Biol Appl. 2019;102:844–62.
3. Fan L, Chen S, Yang M, Liu Y, Liu J. Metallic materials for bone repair. Adv Healthc Mater. 2024;13:e2302132.
4. Gulati K, Chopra D, Kocak-Oztug NA, Verron E. Fit and forget: the future of dental implant therapy via nanotechnology. Adv Drug Deliv Rev. 2023;199:114900.
5. Rullán PJ, Deren ME, Zhou G, Emara AK, Klika AK, Schiltz NK, Barsoum WK, Koroukian S, Piuzzi NS. The Arthroplasty Surgeon Growth Indicator: A Tool for Monitoring Supply and demand trends in the Orthopaedic Surgeon Workforce from 2020 to 2050. J Bone Joint Surg Am. 2023;105:1038–45.
6. Luo Z, Li Z, Xie Z, Sokolova IM, Song L, Peijnenburg W, Hu M, Wang Y. Rethinking Nano-TiO(2) safety: overview of toxic effects in humans and aquatic animals. Small. 2020;16:e2002019.
7. Zhou Z, Shi Q, Wang J, Chen X, Hao Y, Zhang Y, Wang X. The unfavorable role of titanium particles released from dental implants. Nanotheranostics. 2021;5:321–32.
8. Chen L, Tong Z, Luo H, Qu Y, Gu X, Si M. Titanium particles in peri-implantitis: distribution, pathogenesis and prospects. Int J Oral Sci. 2023;15:49.
9. Zhang T, Sze KY, Peng ZW, Cheung KMC, Lui YF, Wong YW, Kwan KYH, Cheung JPY. Systematic investigation of metallosis associated with magnetically controlled growing rod implantation for early-onset scoliosis. Bone Joint J. 2020;102–b:1375–83.
10. Borys J, Maciejczyk M, Antonowicz B, Sidun J, Świderska M, Zalewska A. Free radical production, inflammation and apoptosis in patients treated with Titanium Mandibular Fixations-An observational study. Front Immunol. 2019;10:2662.
11. Borys J, Maciejczyk M, Antonowicz B, Krętowski A, Waszkiel D, Bortnik P, Czarniecka-Bargłowska K, Kocisz M, Szulimowska J, Czajkowski M et al.

Exposure to Ti4Al4V Titanium Alloy Leads to Redox Abnormalities, Oxidative Stress, and Oxidative Damage in Patients Treated for Mandible Fractures. *Oxid Med Cell Longev* 2018, 2018:3714725.
12. Vasconcelos DM, Santos SG, Lamghari M, Barbosa MA. The two faces of metal ions: from implants rejection to tissue repair/regeneration. Biomaterials. 2016;84:262–75.
13. Lee JH, Kwon JS, Moon SK, Uhm SH, Choi BH, Joo UH, Kim KM, Kim KN. Titanium-Silver Alloy miniplates for Mandibular fixation: in Vitro and in vivo study. J Oral Maxillofac Surg. 2016;74:e16221621–16221612.
14. Balachandran S, Zachariah Z, Fischer A, Mayweg D, Wimmer MA, Raabe D, Herbig M. Atomic Scale Origin of Metal Ion Release from Hip Implant Taper junctions. Adv Sci (Weinh). 2020;7:1903008.
15. Rossi S, Savi M, Mazzola M, Pinelli S, Alinovi R, Gennaccaro L, Pagliaro A, Meraviglia V, Galetti M, Lozano-Garcia O, et al. Subchronic exposure to titanium dioxide nanoparticles modifies cardiac structure and performance in spontaneously hypertensive rats. Part Fibre Toxicol. 2019;16:25.
16. Aijie C, Huimin L, Jia L, Lingling O, Limin W, Junrong W, Xuan L, Xue H, Longquan S. Central neurotoxicity induced by the instillation of ZnO and TiO(2) nanoparticles through the taste nerve pathway. Nanomed (Lond). 2017;12:2453–70.
17. Shelly S, Liraz Zaltsman S, Ben-Gal O, Dayan A, Ganmore I, Shemesh C, Atrakchi D, Garra S, Ravid O, Rand D, et al. Potential neurotoxicity of titanium implants: prospective, in-vivo and in-vitro study. Biomaterials. 2021;276:121039.
18. Baranowska-Wójcik E, Szwajgier D, Oleszczuk P, Winiarska-Mieczan A. Effects of Titanium Dioxide nanoparticles exposure on Human Health-a review. Biol Trace Elem Res. 2020;193:118–29.
19. Scherbart AM, Langer J, Bushmelev A, van Berlo D, Haberzettl P, van Schooten FJ, Schmidt AM, Rose CR, Schins RP, Albrecht C. Contrasting macrophage activation by fine and ultrafine titanium dioxide particles is associated with different uptake mechanisms. Part Fibre Toxicol. 2011;8:31.
20. Zhou Y, Ji J, Ji L, Wang L, Hong F. Respiratory exposure to nano-TiO(2) induces pulmonary toxicity in mice involving reactive free radical-activated TGF-β/Smad/p38MAPK/Wnt pathways. J Biomed Mater Res A. 2019;107:2567–75.
21. Zalewska A, Antonowicz B, Szulimowska J, Zieniewska-Siemieńczuk I, Leśniewska B, Borys J, Zięba S, Kostecka-Sochoń P, Żendzian-Piotrowska M, Lo Giudice R et al. Mitochondrial redox balance of fibroblasts exposed to Ti-6Al-4V Microplates subjected to different types of Anodizing. Int J Mol Sci 2023, 24.
22. Wu RS, Lam II, Clay H, Duong DN, Deo RC, Coughlin SR. A Rapid Method for Directed Gene knockout for screening in G0 zebrafish. Dev Cell. 2018;46:112–e125114.
23. !!!. INVALID CITATION !!! [23].
24. Setyawati MI, Tay CY, Chia SL, Goh SL, Fang W, Neo MJ, Chong HC, Tan SM, Loo SC, Ng KW, et al. Titanium dioxide nanomaterials cause endothelial cell leakiness by disrupting the homophilic interaction of VE-cadherin. Nat Commun. 2013;4:1673.
25. Bernier MC, El Kirat K, Besse M, Morandat S, Vayssade M. Preosteoblasts and fibroblasts respond differently to anatase titanium dioxide nanoparticles: a cytotoxicity and inflammation study. Colloids Surf B Biointerfaces. 2012;90:68–74.
26. Cundy PJ, Antoniou G, Freeman BJC, Cundy WJ. Persistently raised serum Titanium levels after spinal instrumentation in children. Spine (Phila Pa 1976). 2022;47:1241–7.
27. Zhang J, Li G, Qu Y, Guo Z, Zhang S, Li D. Fabrication and hemocompatibility evaluation of a robust honeycomb nanostructure on medical pure Titanium Surface. ACS Appl Mater Interfaces. 2022;14:9807–23.
28. Dong J, Zhang L, Ruan B, Lv Z, Wang H, Wang Y, Jiang Q, Cao W. NRF2 is a critical regulator and therapeutic target of metal implant particle-incurred bone damage. Biomaterials. 2022;288:121742.
29. Harris RM, Williams TD, Waring RH, Hodges NJ. Molecular basis of carcinogenicity of tungsten alloy particles. Toxicol Appl Pharmacol. 2015;283:223–33.
30. Guirro PB, Nunes JHC, Cella PS, Marinello PC, Moura FA, Matos RLN, Bracarense A, Borghi SM, Verri WA Jr., Deminice R. Effect of running exercise on titanium dioxide (TiO(2))-induced chronic arthritis and sarcopenia in mice. A titanium prosthesis loosening injury model study. Life Sci. 2022;297:120472.
31. Yu X, Hong F, Zhang YQ. Cardiac inflammation involving in PKCε or ERK1/2-activated NF-κB signalling pathway in mice following exposure to titanium dioxide nanoparticles. J Hazard Mater. 2016;313:68–77.
32. Zhang J, Wang H, Chen H, Li H, Xu P, Liu B, Zhang Q, Lv C, Song X. ATF3-activated accelerating effect of LINC00941/lncIAPF on fibroblast-to-myofibroblast differentiation by blocking autophagy depending on ELAVL1/HuR in pulmonary fibrosis. Autophagy. 2022;18:2636–55.
33. Madaro L, Passafaro M, Sala D, Etxaniz U, Lugarini F, Proietti D, Alfonsi MV, Nicoletti C, Gatto S, De Bardi M, et al. Denervation-activated STAT3-IL-6 signalling in fibro-adipogenic progenitors promotes myofibres atrophy and fibrosis. Nat Cell Biol. 2018;20:917–27.
34. Xu Y, Hadjiargyrou M, Rafailovich M, Mironava T. Cell-based cytotoxicity assays for engineered nanomaterials safety screening: exposure of adipose derived stromal cells to titanium dioxide nanoparticles. J Nanobiotechnol. 2017;15:50.
35. Forcina L, Miano C, Musarò A. The physiopathologic interplay between stem cells and tissue niche in muscle regeneration and the role of IL-6 on muscle homeostasis and diseases. Cytokine Growth Factor Rev. 2018;41:1–9.
36. Armand L, Dagouassat M, Belade E, Simon-Deckers A, Le Gouvello S, Tharabat C, Duprez C, Andujar P, Pairon JC, Boczkowski J, Lanone S. Titanium dioxide nanoparticles induce matrix metalloprotease 1 in human pulmonary fibroblasts partly via an interleukin-1β-dependent mechanism. Am J Respir Cell Mol Biol. 2013;48:354–63.
37. Li J, Yousefi K, Ding W, Singh J, Shehadeh LA. Osteopontin RNA aptamer can prevent and reverse pressure overload-induced heart failure. Cardiovasc Res. 2017;113:633–43.
38. Lee SW, Won JY, Kim WJ, Lee J, Kim KH, Youn SW, Kim JY, Lee EJ, Kim YJ, Kim KW, Kim HS. Snail as a potential target molecule in cardiac fibrosis: paracrine action of endothelial cells on fibroblasts through snail and CTGF axis. Mol Ther. 2013;21:1767–77.
39. Wei Q, Nakahara F, Asada N, Zhang D, Gao X, Xu C, Alfieri A, Brodin NP, Zimmerman SE, Mar JC, et al. Snai2 maintains bone marrow niche cells by repressing Osteopontin expression. Dev Cell. 2020;53:503–e513505.
40. Sun J, Jin X, Zhang X, Zhang B. HMGA2 knockdown alleviates the progression of nonalcoholic fatty liver disease (NAFLD) by downregulating SNAI2 expression. Cell Signal. 2023;109:110741.
41. Imai K, Ishimoto T, Doke T, Tsuboi T, Watanabe Y, Katsushima K, Suzuki M, Oishi H, Furuhashi K, Ito Y, et al. Long non-coding RNA lnc-CHAF1B-3 promotes renal interstitial fibrosis by regulating EMT-related genes in renal proximal tubular cells. Mol Ther Nucleic Acids. 2023;31:139–50.
42. Duan Y, Li J, Qiu S, Ni S, Cao Y. TCF7/SNAI2/miR-4306 feedback loop promotes hypertrophy of ligamentum flavum. J Transl Med. 2022;20:468.
43. Li K, Tang Z, Song K, Fischer NG, Wang H, Guan Y, Deng Y, Cai H, Hassan SU, Ye Z, Sang T. Multifunctional nanocoating for enhanced titanium implant osseointegration. Colloids Surf B Biointerfaces. 2023;232:113604.
44. Toita R, Kitamura M, Tsuchiya A, Kang JH, Kasahara S. Releasable, Immune-Instructive, Bioinspired Multilayer Coating resists Implant-Induced fibrosis while accelerating tissue repair. Adv Healthc Mater. 2024;13:e2302611.
45. Kumar AM, Adesina AY, Hussein MA, Umoren SA, Ramakrishna S, Saravanan S. Preparation and characterization of Pectin/Polypyrrole based multifunctional coatings on TiNbZr alloy for orthopaedic applications. Carbohydr Polym. 2020;242:116285.
46. Alipal J, Lee TC, Koshy P, Abdullah HZ, Idris MI. Evolution of anodised titanium for implant applications. Heliyon. 2021;7:e07408.
47. Kasai Y, Iida R, Uchida A. Metal concentrations in the serum and hair of patients with titanium alloy spinal implants. Spine (Phila Pa 1976). 2003;28:1320–6.
48. Swiatkowska I, Martin NG, Henckel J, Apthorp H, Hamshere J, Hart AJ. Blood and plasma titanium levels associated with well-functioning hip implants. J Trace Elem Med Biol. 2020;57:9–17.

Publisher's Note